11344 *Biochemistry* **2009,** *48,* 11344–11356
DOI: 10.1021/bi901264v

BIOCHEMISTRY
including biophysical chemistry & molecular biology
Article

Binding of Short Oligonucleotides to RNA: Studies of the Binding of Common RNA Structural Motifs to Isoenergetic Microarrays[†]

Elzbieta Kierzek*

Institute of Bioorganic Chemistry, Polish Academy of Sciences, 60-704 Poznan, Noskowskiego 12/14, Poland

Received July 23, 2009; Revised Manuscript Received October 9, 2009

ABSTRACT: Binding of short oligonucleotides to RNA is important for many biological processes. On the basis of RNAi phenomena, antisense, and ribozyme approaches, it is useful in the inhibition of biological functions. To be considered as potential therapeutics, oligonucleotides must bind strongly and selectively to a complementary fragment of target RNA. Microarray technologies also involve the binding of oligonucleotide probes to DNA or RNA. Herein, the hybridization of common structural motifs of RNA, i.e., hairpins, internal loops, bulges, 3′- and 5′-dangling ends, and pseudoknots to isoenergetic microarray probes is presented. The analysis demonstrates that microarray probes bind to bulges, internal loops, and dangling ends as expected. Probes may also bind to terminal helixes, however, possibly due to the rearrangement of base pairs. These results suggest that isoenergetic microarray mapping can provide data to facilitate and improve RNA secondary structure prediction. However, optimal results require combination with chemical and/or enzymatic mapping.

RNA plays a major role in biological processes, and knowledge about the structure of RNA is crucial for understanding its functions. The secondary structure of RNA is formed from common structural motifs such as double helixes, hairpins, bulges, internal loops, multibranch loops, pseudoknots, dangling ends, and single stranded regions (*1*). Single stranded regions are good targets for the binding of complementary oligonucleotides, which can be designed to disturb or control the biological functions of RNA (*2*). Differently modified nucleotides are widely used to enhance the stability of duplexes (*3*, *4*). It is therefore important to advance the knowledge of the binding of modified short oligonucleotides to folded RNA. Nearest neighbor thermodynamic parameters for RNA (*5*, *6*), DNA (*7*), DNA/RNA (*8*), and 2′-*O*-methyl-RNA/RNA (*9*) as well as chimeric locked nucleic acids (LNA[1])-DNA/DNA (*10*) and LNA-2′-*O*-methyl RNA/RNA (*11*, *12*) duplexes were published and allow for predictions of the thermodynamic stability of respective duplexes. Hybridization of structural motifs of RNA to modified probes spotted on microarrays gives opportunities to study their binding to short modified oligonucleotides. Those results can also facilitate the design of oligonucleotides as potential therapeutics.

Recently, microarrays with 2′-*O*-methyl penta/hexanucleotide isoenergetic probes were used for the study of the secondary structure of target RNAs and together with the RNAstructure computer program (*13*) improved prediction of RNA folding (*14*−*16*). Isoenergetic microarrays are built with LNA-2′-*O*-methyl RNA chimeric oligonucleotides. LNA modified nucleotides C, G, and U as well as LNA-2,6-diaminopurine riboside and/or 2′-*O*-methyl-2,6-diaminopurine riboside substituting for adenosine were applied in isoenergetic microarray preparation (*15*, *17*). Probes are isoenergetic because their modifications were designed to provide roughly equally favorable and enhanced free energy of binding to complementary single stranded fragments of target RNA. The position and type of modified nucleotides were selected on the basis of thermodynamic rules determined previously (*9*, *11*, *12*, *18*). The main advantage of isoenergetic probes is the independence of their binding on base content and sequence. This significantly facilitates interpretation of the hybridization results. The presence of LNA and 2,6-diaminopurine riboside nucleotides results in strong enhancement of probe binding; thus, short penta/hexanucleotides can serve as isoenergetic probes. The small number of possible pentamers (only 1024) allows for the production of universal isoenergetic microarrays suitable to investigate the structure of any RNA. A disadvantage of short probes is the increased probability of having more than one perfect matched site in target RNA. A microarray mapping method has been used to study the structures of natural RNAs. This method identifies single stranded or weakly paired regions in target RNA and improves predictions of the target secondary structure. A microarray mapping method was used to improve the secondary structure prediction of 5S rRNA from *Escherichia coli* from 27% to 92% (*14*). Isoenergetic microarray mapping was applied to model the secondary structures of R2 5′RNAs from *Bombyx mori*, *Samia cynthia*, *Coscinocera hercules*, *Callosamia promethea*, and *Saturnia pyri* (*15*, *16*). Those, RNAs of 320−330 nucleotides have similar biological functions and reveal several common structural motifs. Isoenergetic microarray mapping potential was investigated on tRNAs as well. Binding of probes to natural $tRNA^{Phe}$ from *Saccharomyces cerevisiae* and to the unmodified transcript was determined to reveal the influence of tRNA modification on binding (*19*). Also, the comparison of microarray hybridization of initiator $tRNA_i^{Met}$ and elongator $tRNA_m^{Met}$ from *Lupinus luteus* demonstrated differences in the folding of

[†]This work was supported by Ministry of Science and Higher Education Grant N N301 3383 33 (to E.K.) and PBZ-MNiSW-07/1/2007 (to Ryszard Kierzek).

*To whom correspondence should be addressed. Phone: +48-61 852-85-03. Fax: +48-61 852-05-32. E-mail: Elzbieta.Kierzek@ibch.poznan.pl.

[1]Abbreviations: LNA, locked nucleic acids; Na_2EDTA, ethylenediaminetetraacetic acid disodium salt; rRNA, ribosomal ribonucleic acid; tRNA, transfer ribonucleic acid; NMR, nuclear magnetic resonance.

 Published on Web 10/17/2009

both molecules, which could be related to their biological functions during elongation (*20*).

Not much is known about the thermodynamics of binding of short oligonucleotides to folded RNA (*21*−*25*). Systematic studies of microarray mapping of common RNA structural motifs are important to improve the interpretation of hybridization results with large RNA. In this article, hybridization results for many model short RNAs with defined structure are presented. Model RNAs were designed to represent the most common structural motifs of RNA, i.e., hairpins, internal loops, bulges, 3′- and 5′-dangling ends, and pseudoknots.

MATERIALS AND METHODS

Materials. Standard phosphoramidites for oligonucleotide synthesis and C6-aminolinker were purchased from Glen Research. Phosphoramidites of LNA, LNA-2,6-diaminopurine riboside, and 2′-*O*-methyl-2,6-diaminopurine riboside were synthesized as described previously (*11*).

The γ^{32}P-ATP was purchased from ICN Biomedicals, and T4 polynucleotide kinase and T4 RNA ligase were from Fermentas. Ap and Cp for the synthesis of ^{32}P labeled pAp and ^{32}P labeled pCp, respectively, were from Sigma. RNases V1 and T1 were from Ambion and nuclease S1 from Fermentas. Dimethyl sulfate (DMS) and 1-cyclohexyl-3-(2-morpholinoethyl)carbodiimide metho-*p*-toluenesulfonate (CMCT) were from Aldrich, and kethoxal was from ICN Biomedicals. *N*-Methylisatoic anhydride (NMIA) was from Molecular Probes. Reverse transcriptase SuperScript III was from Invitrogen and dNTPs and ddNTPs from Amersham Biosciences. Lead(II) acetate was purchased from Fluka.

HybriSlip hybridization covers and agarose were from Invitrogen. Silanized slides were purchased from Sigma. Humidity-temperature chambers for hybridization were manufactured in-house.

Chemical Synthesis of Model RNA and Modified Oligonucleotide Probes. Oligonucleotides probes and short model RNA were synthesized by the phosphoramidite approach on an ABI 392 synthesizer (*26*). LNA phosphoramidites were synthesized as described before (*27*). The modified oligonucleotides used as probes for microarrays were synthesized with a C6-aminolinker on the 5′-end. Oligonucleotides were deprotected and purified according to published procedures (*5*, *15*).

Molecular weights were confirmed by mass spectrometry (LC MS Hewlett-Packard series 1100 MSD with API-ES or MALDI TOF MS, model Autoflex, Bruker). Concentrations of all oligonucleotides were determined from predicted extinction coefficients for RNA (*28*) and measured absorbance at 260 nm at 80 °C. It was assumed that modified 2′-*O*-methyl RNA and RNA strands with identical sequences have identical extinction coefficients.

Synthesis of 74-Nucleotide Fragment of B. mori R2 Retrotransposon 5′ Region. The plasmid for the synthesis of 74-nucleotide RNA (Pk2), a fragment of *B. mori* R2 retrotransposon, was a gift from James M. Hart and Dr. Douglas H. Turner. The plasmid was linearized and transcribed according to a published procedure (*29*). Synthesized Pk2 RNA was purified on an 8% polyacrylamide denaturing gel.

Native gel electrophoresis (8% polyacrylamide gel, run at 4 °C) was done for Pk2 after folding for 5 min at 65 °C in buffers (A) 200 mM NaCl, 5 mM $MgCl_2$, and 10 mM Tris-HCl at pH 8.0 or (B) 1 M NaCl, 5 mM $MgCl_2$, and 10 mM Tris-HCl at pH 8.0. In both conditions, Pk2 RNA migrated as one and the same band.

Preparation of Isoenergetic Microarrays. Isoenergetic microarray probes were designed and synthetized as described earlier (*14*, *15*). They were built with 2′-*O*-methyl oligonucleotide pentamers and hexamers with incorporated LNA nucleotides and 2,6-diaminopurine ribosides (LNA or 2′-*O*-methyl). Modifications were chosen to provide predicted free energies for binding at 37 °C ($\Delta G°_{37}$) to unstructured RNA of between −8.0 and −10.5 kcal/mol. The sequence UUUUU and spotting buffer were used as negative controls. Microarrays were prepared according to the method described earlier (*15*, *30*). Silanized slides were coated with 2% agarose activated by $NaIO_4$, and probes were spotted in 4 or 6 repeats by a microarray printer (SpotArray 24, Perkin-Elmer Life Sciences) with a spot distance of 750 μm. Microarrays contained all probes complementary step-by-step to the sequences of all model RNAs from Figures 1 and 2. Other microarrays, with probes step-by-step complementary to Pk2 (Figure 3), were printed separately. Printed microarrays were incubated for 12 h at 37 °C in 100% humidity. The remaining aldehyde groups on microarrays were reduced with 35 mM $NaBH_4$ solution in PBS buffer (137 mM NaCl, 2.7 mM KCl, 4.3 mM Na_2HPO_4, and 1.4 mM KH_2PO_4 at pH 7.5) and ethanol (3:1 v/v). Then slides were washed in water at room temperature (3 washes for 30 min each), in 1% SDS solution at 55 °C for 1 h, and finally in water at room temperature (3 washes for 30 min each), and dried at room temperature overnight.

Labeling of Target RNA. RNA prior to hybridization was 5′-end labeled using γ^{32}P-ATP and T4 polynucleotide kinase. Pk2 was also 5′-end ^{32}P labeled for enzymatic and lead cleavage. Additionally, 3′-end ^{32}P labeling was accomplished with pAp and pCp for some cases, as indicated.

Hybridization on Isoenergetic Microarrays. Prior to hybridization, RNA was radioactively labeled from the 5′- or 3′-end and purified on a denaturing gel. The following buffers were used for hybridization: (A) 200 mM NaCl, 5 mM $MgCl_2$, and 10 mM Tris-HCl at pH 8.0, (B) 1 M NaCl, 5 mM $MgCl_2$, and 10 mM Tris-HCl at pH 8.0, and (C) 1 M NaCl, 20 mM sodium cacodylate, and 0.5 mM Na_2EDTA at pH 7.0. RNAs were folded in one of the above buffers by incubation for 5 min at 65 °C and slowly cooling to room temperature. For hybridization, ca. 10 nM of ^{32}P labeled RNA in 250 μL of folding buffer was placed on a microarray slide and covered with a HybriSlip. The microarray slide was placed in a humidity-temperature chamber with 100% humidity and incubated for 18 h at 4 °C. After hybridization, buffers with RNA were poured out, and slides were washed in buffer with the same salt concentrations for 3 min at 0 °C. Different hybridization times (4 h, 8 h) and temperatures (4 °C, room temperature, 37 °C) and also various washing times (1, 3, 10, and 15 min at 0 °C) were also tested. Slides were dried by centrifugation in a clinical centrifuge (2000 rpm, 2 min) and covered with plastic wrap. Hybridization was visualized by exposure to a phosphorimager screen and scanned on Molecular Dynamics or Fuji Phosphorimagers. Quantitative analysis was performed with ImageQuant 5.2. Binding was considered strong, medium, or weak when the integrated intensity was ≥1/3, ≥ 1/9, or ≥1/27 of the strongest integrated intensity, respectively. Experiments were repeated at least three times, and the average of the data is presented.

Thermodynamic Measurements. Oligonucleotides were melted in buffer D containing 10 mM NaCl, 20 mM sodium cacodylate, and 0.5 mM Na_2EDTA at pH 7.0. Low NaCl concentration was chosen to keep melting temperatures in a measurable range. However, several low stability duplexes were

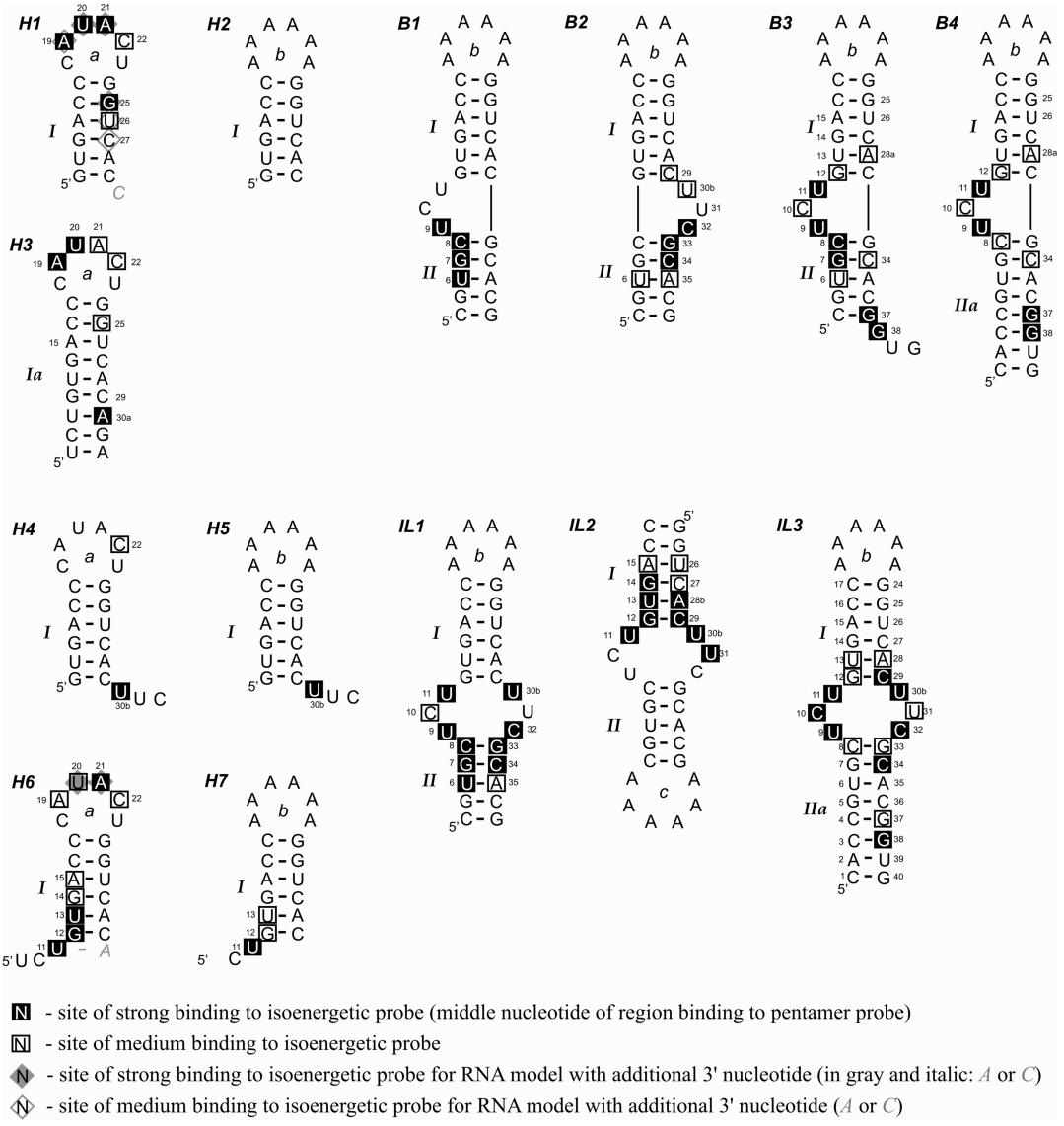

FIGURE 1: Secondary structures and hybridization results of model RNA motifs: hairpins, bulges, internal loops, and 3′- and 5′-dangling ends. Each RNA was hybridized to a microarray with all possible isoenergetic probes, complementary step-by-step to RNA. Pentamer probes are 6, 7, 16, 29, 34, 35, and 38. All other probes used are hexamers with specific pentamer sequence complementary to target RNA and unspecific G^L on the 3′-end (Tables 1 and 2, Supporting Information). The numbering of nucleotides in each structure is according to the longest RNA (IL3) to show similarity in sequence and for easier comparison.

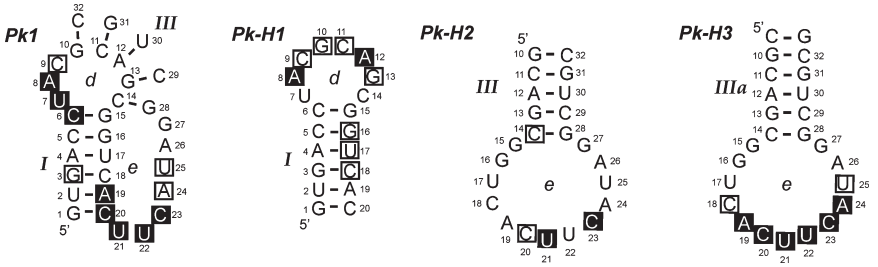

FIGURE 2: Secondary structures and hybridization results of model RNA pseudoknot Pk1 and its hairpins as parts of the pseudoknot structure. Each RNA was hybridized to a microarray with all possible isoenergetic probes, complementary step-by-step to RNA. Pentamer probes are 14, 15, 16, 29, and 30b. All other probes used are hexamers with the specific pentamer sequence complementary to target RNA and unspecific G^L on 3′-end (Table 3, Supporting Information). The numbering of nucleotides is used according to pseudoknot Pk1. For symbols, refer to Figure 1.

melted in buffer C containing 1 M NaCl, 20 mM sodium cacodylate, and 0.5 mM Na_2EDTA at pH 7.0. Absorbance vs temperature melting curves were measured at 260 nm with a heating rate of 1 °C/min from 0 to 90 °C on a Beckman DU 640 spectrometer with a water cooled Peltier thermoprogrammer. Melting curves were analyzed, and thermodynamic parameters were calculated with the program MeltWin 3.5 (*31*).

Enzymatic, Chemical Mapping, and Lead Cleavages. Structural mapping of R2 pseudoknot (Pk2) was conducted according to published procedures (*14*, *15*, *32*−*34*). Chemical

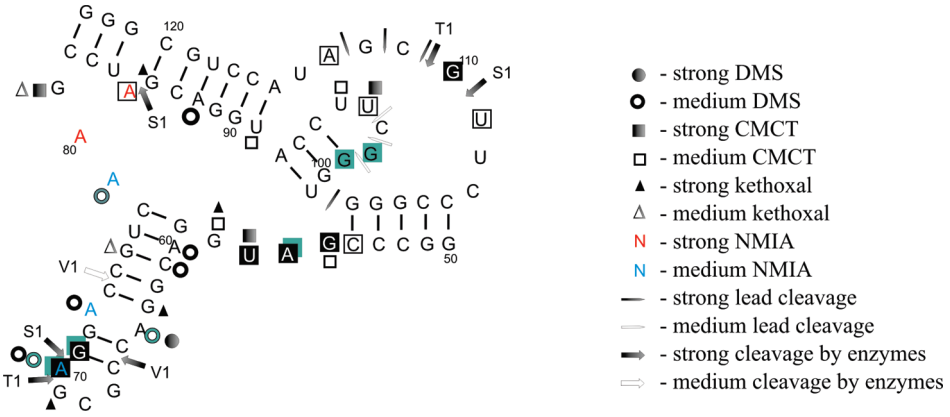

FIGURE 3: Secondary structure and hybridization results for 74-nucleotide pseudoknot (Pk2), a part of *B. mori* R2 5′RNA. Data shown are for buffer (A) (200 mM NaCl, 5 mM $MgCl_2$, and 10 mM Tris-HCl at pH 8.0) at room temperature. Pk2 was hybridized to a microarray with all possible isoenergetic probes complementary to Pk2. Pentamer probes are 52, 53, 63, 64 (73), 65 (74), 67, 76, 88, 98−107, 118, 120, and 121. The other probes are hexamers with the 5′ pentamer sequence complementary to Pk2 and G^L on the 3′-end (Table 4, Supporting Information). The numbering is according to *B. mori* R2 5′RNA. Previously used symbols are described in Figure 1. Symbols in green: chemical mapping or strong binding to the microarray probe in *B. mori* R2 5′RNA.

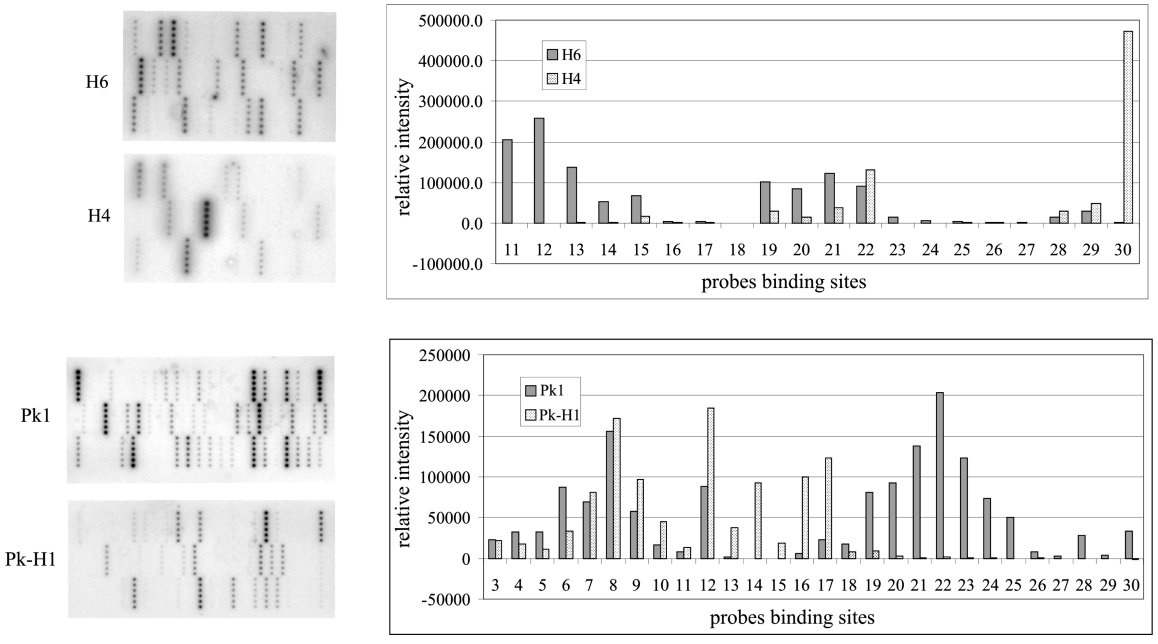

FIGURE 4: Examples of hybridization results for model RNAs. Upper panel: microarrays with hybridized hairpins H4 and H6 along with the bar graph of relative binding intensity to the probes. Lower panel: microarrays and bar graph for Pk1 and Pk-H1. Each probe was spotted six times, and the average intensity is plotted.

mapping was done with DMS, CMCT, kethoxal, and NMIA followed by primer extension for readout. The DNA for primer extension was complementary to nucleotides 97 to 123 of Pk2.

RESULTS

To take full advantage of data collected from hybridization on isoenergetic microarrays, it is useful to test the microarray mapping of small model RNAs with defined secondary structure. Model RNAs were designed as representatives of the structural motifs such as hairpins, internal loops, bulges, 5′- and 3′-dangling ends, and pseudoknots (Figures 1−3). In the first group of model RNAs, the hairpins H1 and H2 were extended to form additional structural motifs (Figure 1). This strategy allows for a systematic analysis of the influence of RNA structure on binding to isoenergetic microarray probes. To unify the analysis, the nucleotides are numbered in accordance with their positions in the longest RNA model. Hybridization results are shown in Figures 1−4 and listed in Tables 1−3. Only strong and medium binding sites were used for analysis. On average, the predicted free energy of binding unstructured RNA to the probes (ΔG°_{37}) is −11.7 kcal/mol in 0.1 M NaCl. Probes that bound were checked for alternative binding sites with the bimolecular binding mode of RNAstructure 4.5 (*13*). Hybridization experiments were performed mostly in buffer C containing 1 M NaCl as described in Materials and Methods. This condition provided the strongest binding. Hybridizations performed in buffers A and B gave relative intensities of binding similar to those in buffer C, but overall signals were weaker. For short model RNA targets, shorter hybridization time, higher temperature, and longer washing decrease intensities of all microarray spots, but relative intensities remain similar. Complete hybridization results are presented in Supporting Information.

Binding of RNA Hairpins to Isoenergetic Microarray Probes. Figure 1 shows the hairpins investigated, and Tables 1

Table 1: Hybridization Results for RNA H1−H7[a]

center of binding site[b]	sequence of modified probe 5′ to 3′[c]	added 3′ base pair	predicted ΔG°_{37} (modified probe/RNA in 0.1 M NaCl)[d]		binding of isoenergetic probes[e]						
				with dangling ends of target RNA[f]	H1 (H1−3′C)	H3	H4	H6 (H6−3′A)	H2	H5	H7
11	$D^{L}CD^{L}GD^{L}G^{L}$	dangling G^{L}	−9.13	−9.83				S			S
12	$CD^{L}CD^{L}GG^{L}$	U-G^{L}	−8.98	−10.08				S			M
13	$U^{L}CD^{L}CD^{L}G^{L}$	C-G^{L}	−10.85	−11.45				S			M
14	$GUC^{L}DC^{L}G^{L}$	U-G^{L}	−8.89	−9.99				M			
15	$GG^{L}UC^{L}DG^{L}$	G-G^{L}	−10.25	−11.15				M			
17	$UG^{L}GG^{L}UG^{L}$	G-G^{L}	−10.63	−11.33					S[g]		
19	$UD^{L}UG^{L}GG^{L}$	C-G^{L}	−11.48	−12.48	S (M)	S		M			
20	$G^{L}UD^{L}UG^{L}G^{L}$	C-G^{L}	−11.61	−13.11	S (S)	S		M (S)			
21	$DG^{L}UD^{L}UG^{L}$	C-G^{L}	−10.52	−11.52	S (S)	M		S (S)			
22	$CD^{L}GU^{L}DG^{L}$	A-G^{L}	−8.82	−10.42	M	M	M	M			
25	$GDC^{L}CAG^{L}$	C-G^{L}	−10.19	−12.39	S (S)	M			S[g]		
26	$UG^{L}AC^{L}CG^{L}$	U-G^{L}	−9.50	−10.30	M (M)						
27	$GU^{L}GD^{L}CG^{L}$	G-G^{L}	−9.19	−9.29 (−10.09)	(M)						
30a	$UC^{L}UG^{L}UG^{L}$	C-G^{L}	−10.91	−11.01		S					
30b	$GD^{L}DG^{L}UG^{L}$	C-G^{L}	−11.17	−11.27			S			S	

[a]Only probes that bind strongly or moderately to at least one target RNA are shown. [b]Center of binding site according to Figure 1, where the center is the target RNA nucleotide complementary to the third nucleotide from the 5′-end of the probe. [c]In sequence of the modified probe: LNA nucleotides are marked with superscript ^{L}; D represents 2,6-diaminopurine riboside; and nucleotides without a superscript are 2′-*O*-methyl-nucleotides. [d]Calculated for 100 mM NaCl buffer according to a published equation (*15*). [e]Buffer composition: 1 M NaCl, 20 mM sodium cacodylate, and 0.5 mM Na_2EDTA at pH 7 (buffer C). [f]Calculated for target RNA which binds the probe. Symbols: S, strong binding; M, medium binding. [g]Strong binding is relatively weaker (70−100 times) compared to that of other target RNAs.

Table 2: Hybridization Results for RNA B1−B4 and IL1-IL3[a]

center of binding site[b]	sequence of modified probe 5′ to 3′[c]	added 3′ base pair	predicted ΔG°_{37} (modified probe/RNA in 0.1 M NaCl)[d]		binding of isoenergetic probes[e]						
				with dangling ends of target RNA[f]	B1	B2	B3	B4	IL1	IL2	IL3
6	$GCD^{L}CG^{L}$		−8.42	−9.62 B1, B3, IL1; −10.12 B2	S	M	M		S		
7	$AG^{L}CD^{L}CG^{L}$	C-G^{L}	−11.48	−11.58	S		S		S		
8	$GD^{L}GCD^{L}G^{L}$	G-G^{L}	−10.44	−11.94	S		S	M	S		M
9	$D^{L}GD^{L}GCG^{L}$	U-G^{L}	−10.04	−10.94	S		S	S	S		S
10	$CD^{L}GD^{L}GG^{L}$	G-G^{L}	−9.86	−10.56			M	M	M		S
11	$D^{L}CD^{L}GD^{L}G^{L}$	C-G^{L}	−11.96	−12.86			S	S	S	S	S
12	$CD^{L}CD^{L}GG^{L}$	U-G^{L}	−8.98	−10.38			M	M		S	M
13	$U^{L}CD^{L}CD^{L}G^{L}$	C-G^{L}	−10.85	−11.45						S	M
14	$GUC^{L}DC^{L}G^{L}$	U-G^{L}	−8.89	−9.99						S	
15	$GG^{L}UC^{L}DG^{L}$	G-G^{L}	−10.25	−10.35						M	
26	$UG^{L}AC^{L}CG^{L}$	dangling G^{L}	−8.80	−9.30						M	
27	$GU^{L}GD^{L}CG^{L}$	G-G^{L}	−9.19	−10.39						M	
28b	$D^{L}GU^{L}GD^{L}G^{L}$	G-G^{L}	−10.06	−10.39						S	M
28a	$CG^{L}UG^{L}DG^{L}$	G-G^{L}	−10.24	−10.84			M[i]	M			
29	$D^{L}DG^{L}UG^{L}G^{L}$	U-G^{L}	−9.44	−9.74		M[g]				S	S
30b	$GD^{L}DG^{L}UG^{L}$	C-G^{L}	−11.17	−12.97		M			S	S	S
31	$CGD^{L}DG^{L}G^{L}$	A-G^{L}	−9.32	−10.02						S	M
32	$GC^{L}GD^{L}AG^{L}$	C-G^{L}	−11.62	−13.82		S			S		S
33	$UGC^{L}GD^{L}G^{L}$	U-G^{L}	−10.42	−11.22		S			S		M
34	$G^{L}UG^{L}CG^{L}$		−9.48	−11.68 B3, B4; −11.28 B2, IL1, IL3		S[h]	M[j]	M	S[h]		S
35	$CG^{L}UG^{L}CG^{L}$	C-G^{L}	−12.88	−12.98		M[h]			M[h]		
37	$DC^{L}CG^{L}UG^{L}$	C-G^{L}	−12.20	−13.10			S[k]	S			M
38	$C^{L}DC^{L}CG^{L}$		−9.02	−9.32			S	S			S

[a]Only probes that bind strongly or moderately to at least one target RNA are shown. [b]Center of binding site according to Figure 1, where the center is the target RNA nucleotide complementary to the third nucleotide from the 5′-end of the probe. [c]In sequence of the modified probe: LNA nucleotides are marked with superscript ^{L}; D represents 2,6-diaminopurine riboside; and nucleotides without a superscript are 2′-*O*-methyl-nucleotides. [d]Calculated for 100 mM NaCl buffer according to a published equation (*15*). [e]Buffer composition: 1 M NaCl, 20 mM sodium cacodylate, and 0.5 mM Na_2EDTA at pH 7 (buffer C). [f]Calculated for target RNA which binds the probe. Symbols: S, strong binding; M, medium binding. [g]Possible alternative binding sites: 35, 33. [h]Possible alternative binding sites: 6. [i]Possible alternative binding sites: 38/39. [j]Possible alternative binding sites: 9. [k]Possible alternative binding sites: 28/29.

Table 3: Hybridization Results for RNA Pk1, Pk-H1, Pk-H2, and Pk-H3[a]

center of binding site[b]	sequence of modified probe 5′ to 3′[c]	added 3′ base pair	predicted $\Delta G°_{37}$ (modified probe/RNA in 0.1 M NaCl)[d]		binding isoenergetic probes[e]			
				with dangling ends of target RNA[f]	Pk1	Pk-H1	Pk-H2	Pk-H3
3	$GUC^{L}DC^{L}G^{L}$	dangling G^{L}	−8.19	−8.99	M			
6	$UD^{L}GG^{L}UG^{L}$	G-G^{L}	−9.44	−10.04	S[g]			
7	$G^{L}UD^{L}GG^{L}G^{L}$	A-G^{L}	−10.16	−12.06	S			
8	$CG^{L}UD^{L}GG^{L}$	C-G^{L}	−12.06	−12.96	S	S		
9	$GC^{L}GU^{L}AG^{L}$	C-G^{L}	−11.17	−13.17	M	M		
10	$U^{L}GC^{L}GU^{L}G^{L}$	U-G^{L}	−9.35	−10.45		M		
11	$CU^{L}GC^{L}GG^{L}$	A-G^{L}	−10.48	−10.98		M		
12	$GC^{L}UG^{L}CG^{L}$	C-G^{L}	−13.49	−15.69		S		
13	$CG^{L}CU^{L}GG^{L}$	G-G^{L}	−10.48	−12.08		M		
14	$CC^{L}GC^{L}U$		−9.88	−10.78			M	
16	$GDC^{L}CG^{L}$	G-G^{L}	−8.92	−11.12		M		
17	$UG^{L}AC^{L}CG^{L}$	C-G^{L}	−11.58	−12.28		M		
18	$GU^{L}GD^{L}CG^{L}$	G-G^{L}	−9.19	−10.69 Pk-H1; −9.49 Pk-H3		M		M
19	$D^{L}GU^{L}GD^{L}G^{L}$	G-G^{L}	−10.06	−10.36	S			S
20	$D^{L}DG^{L}UG^{L}G^{L}$	U-G^{L}	−9.44	−9.74	S[h]		M	S
21	$GD^{L}DG^{L}UG^{L}$	C-G^{L}	−11.17	−12.97	S		S	S
22	$U^{L}GD^{L}DG^{L}G^{L}$	A-G^{L}	−9.17	−10.07	S			S
23	$D^{L}UG^{L}DD^{L}G^{L}$	C-G^{L}	−11.24	−12.44	S		S	S
24	$UD^{L}UG^{L}DG^{L}$	U-G^{L}	−8.47	−9.57	M			S
25	$C^{L}UD^{L}UG^{L}G^{L}$	U-G^{L}	−8.66	−10.06	M			M

[a]Only probes that bind strongly or moderately to at least one target RNA are shown. [b]Center of binding site according to Figure 1, where the center is the target RNA nucleotide complementary to the third nucleotide from the 5′-end of the probe. [c]In sequence of the modified probe: LNA nucleotides are marked with superscript ^{L}; D represents 2,6-diaminopurine riboside; and nucleotides without a superscript are 2′-*O*-methyl-nucleotides. [d]Calculated for 100 mM NaCl buffer according to a published equation (*15*). [e]Buffer composition: 1 M NaCl, 20 mM sodium cacodylate, and 0.5 mM Na_2EDTA at pH 7 (buffer C). [f]Calculated for target RNA which binds the probe. Symbols: S, strong binding; M, medium binding. [g]Possible alternative binding sites: 20. [h]Possible alternative binding sites: 7/8.

and 2 list the results. For hairpin H1, strong binding was only expected in loop *a*. Indeed, binding to the loop at positions 19−21 (strong) and 22 (medium) was observed, but binding to sites 25 (strong) and 26 (medium) was also noticed. In hairpin H2, loop *b* was built with six A nucleotides to limit possibilities for binding with mismatched probes. Probe UUUUU was printed on each microarray as a negative control because the binding constant for five AU base pairs is too low to retain RNA on the microarray. Indeed, no strong or medium binding was detected for hairpin H2. Weak binding was observed at sites 25 and 17. The strength of the strongest binding site, 17, is 70 times weaker than the strongest binding site: site 19 of hairpin H1. Moreover, the probe complementary to site 25 had a binding signal 100 times weaker for hairpin H2 than for hairpin H1. Hairpin H3, with loop *a*, has helix I extended by three base pairs (Ia). Hybridization results show binding to loop *a*, at positions 19−22, similar to the binding in hairpin H1. Medium binding is observed at site 25, which is weaker than that for H1. Surprisingly, site 30a in helix Ia binds strongly.

Hairpins with a 3′-dangling end, H4 and H5, bind very strongly at site 30b in the unpaired end, but the only binding in loop *a* is medium at site 22. This weak binding in H4 loop *a* compared to that in H1 is surprising. The big difference could come from the relatively small concentration of RNA compared to concentrations of probes on the microarrays. Increasing the concentration of H4 by 10-fold changed the results. Site 30b retained strong binding, site 22 increased to strong binding, and sites 21 and 25 increased to medium binding. As expected, hairpin H5 with six A nucleotides in loop *b* binds strongly only at position 30b.

Hairpins with a 5′-dangling end, H6 and H7, have a different pattern of binding to microarrays (Figures 1 and 4). In H6, there was strong or medium binding to sites 11−15 as well as strong or medium binding to positions 19−22 in loop *a*. Similarly, probes for positions 11−13 on hairpin H7 also bind. Evidently, the 5′-dangling ends facilitate the binding of the probes to the 5′-end of helix I. Those hybridization results are consistent with measured thermodynamic data (Table 5).

To see if binding to H6 helix I required an unpaired U11, ligation with ^{32}P labeled pAp was used to allow U11 to form a U11-A30 base pair (Figure 1, structure H6 including gray *A*; binding results marked in gray). In this case, only strong binding was observed at sites 20 and 21. Evidently, extending helix I by one base to pair U11 with A30 eliminated the binding of probes to helix I.

Binding of RNA Bulges and Internal Loops to Isoenergetic Microarray Probes. Hairpins H1, H5, and H7 were expanded to include a bulge of three nucleotides or a 3 × 3 nucleotide internal loop (Figure 1). Thermodynamic stabilities of the RNAs were also measured (Table 5).

For sequence B1 with a bulge on the 5′ side, strong binding was detected in the bulge loop at position 9 and also in the 5′-adjacent region, at positions 6−8. Helix I and the 3′-side of helix II in B1 did not bind probes. B2 with the bulge loop on the 3′ side exhibited binding in the bulge loop, at 30b and 32, and on the 3′-side of helix II at positions 33 to 35, which are 3′-adjacent to the bulge loop. Except for medium binding at positions 6 and 29, helix I and the strand in helix II opposite to the bulge loop did not bind probes. Evidently, bulge loops in RNA facilitate probe binding to an adjacent strand in a terminal helix. B3 exhibited strong binding at sites 7−9 and medium binding at site 6, which is similar to B1. There is new strong binding at site 11 and medium binding at sites 10 and 12 relative to B1 and 28a, which differs from B1, however. Strong binding also occurred at the 3′-dangling end

Table 4: Hybridization Results for Pk2[a]

center of binding site[b]	sequence of modified probe 5′ to 3′[c]	added 3′ base pair	predicted $\Delta G°_{37}$ (modified probe/RNA in 0.1 M NaCl)[d]		binding RT 200 mM NaCl, 5 mM $MgCl_2$[f]	binding RT 1 M NaCl, 5 mM $MgCl_2$[f]	binding 4 °C 200 mM NaCl, 5 mM $MgCl_2$[f]	binding 4 °C 1 M NaCl, 5 mM $MgCl_2$[f]	$\Delta G°_{37}$ predicted (kcal/mol) for complement binding (no structure of Pk2 RNA)[g]	$\Delta G°_{37}$ predicted (kcal/mol) for alternative binding site[g,h,i]	alternative binding site[g,h,i]	probable binding sites[h]
				with dangling ends of target RNA[e]								
54	$U^LCG^LGG^L$		−9.69	−10.49	M	M	M	M	−7.6	−4.3; −4.1	66/67; 106	54
55	$DU^LCG^LGG^L$	G^L-C	−12.43	−13.33	S	S	S	S	−8.8			55
56	$CD^LUC^LGG^L$	G^L-C	−11.63	−13.23	S (S)	S (S)	(S)	S	−8.8	(−7.4)	(6)	56 (56)
57	$CCD^LUC^LG^L$	G^L-C	−11.59	−12.99	S	S	S	S				57
60	$CG^LUC^LCG^L$	G^L-U	−10.57	−12.37	(S)						(many)	(122/123; 238/239)
61	$CC^LGU^LCG^L$	G^L-G	−10.27	−11.47	M			M	−9.0	−8.2; −5.4	56/57; 120/121	56
63	$G^LUC^LCG^L$		−9.25	−10.55		(S)				(−7.5; −7.2; −7.2; −6.7; −6.3; −6.3)	(122; 59/60; 238/239; 59; 307/308; 72/73)	(122; 238/239)
70	$CC^LUC^LGG^L$	G^L-G	−10.55	−11.95	M (S)	M (S)	M (S)	M (S)	−8.6	−7.0; (−7.2)	56; (262)	70; 56; (70; 56)
71	$U^LCC^LUC^LG^L$	G^L-C	−12.42	−13.12	S (S)	S (S)	M (S)	S	−8.7	(−7.8; −6.1)	(237; 262)	71; (71; 237)
72	$GUC^LCU^LG^L$	G^L-G	−8.67	−9.77		(S)			−7.4	(−8.3; −7.5; −6.7; −6.4; −6.3; −6.0)	(238; 292/293; 59/60; 104; 122/123; 63/64)	(238; 122/123)
85	$GC^LUD^LGG^L$	G^L-C	−12.67	−14.57	M		(S)		−10.0	(−6.8; −6.7)	(215; 301/302)	85; (85; 215 301/302)
86	$U^LGC^LUD^LG^L$	G^L-C	−12.02	−13.12			(S)		−7.5			(86)
88	CC^LUG^LC		−9.74	−10.84			(S)		−7.6	(−7.4; −6.5)	(261; 121)	(261; 121)
89	$D^LCC^LUG^LG^L$	G^L-G	−10.28	−11.48	(S)				−7.2	(−6.6; −6.3; −6.1)	(99; 98/99; 241/242)	(99; 98/99; 241/242)
91	$GUD^LCC^LG^L$	G^L-A	−9.14	−10.24				(S)	−7.4			(91)
96	$CGD^LDG^LG^L$	G^L-C	−12.25	−14.05	M			M	−8.8	−4.6	108/109	96; 109
98	CCC^LGA		−8.05	−8.75	(S)	(S)	(S)	(S)	−7.6	(−7.6; −7.5; −6.6)	(138; 261/262; 121/122)	(98)
99	ACC^LCG^L		−8.79	−9.59	(S)	(S)	(S)	(S)	−7.4	(−6.8; −6.7; −6.2; −6.0)	(139; 261/262; 121/122; 263/264)	(99)
100	CD^LCC^LC		−9.06	−9.66		(S)			−8.4			(100)
102	CCC^LDC		−7.72	−8.32		(S)	(S)	(S)	−8.1	(−7.6; −7.4)	(160; 286)	(160; 286)
105	$GGGCC^L$		−9.41	−10.71	(S)	(S)	(S)		−10.9	(−10.4; −8.7; −8.2; −7.9; −7.9; −7.4)	(105; 152/153; 288; 216/217; 122/123; 104/105)	(105; 3)
109	$GC^LDD^LGG^L$	G^L-C	−12.45	−14.45	M	S	M	S	−9.7	−5.6; −5.4	118; 84	109
110	$CG^LCD^LDG^L$	G^L-C	−11.95	−13.35	S	S	M	S	−8.2	−5.6; −4.5	119/120; 68	110
111	$UC^LGCD^LG^L$	G^L-U	−9.93	−10.83			M	S	−6.8	−8.0	119/120	111
113	$UD^LUC^LGG^L$	G^L-G	−8.34	−8.94	M		M	S	−4.5	−6.7	55/56	113; 55; 56
117	$CD^LGG^LUG^L$	G^L-U	−10.15	−11.05			M	M	−6.8	−4.3; −4.3	82/83; 93	117
118	GCD^LGG^L		−9.37	−11.57	M			S	−9.0	−6.1; −5.4; −4.9	109; 108; 84	109
119	$CG^LCD^LGG^L$	G^L-C	−13.30	−15.10	S	S	M	S	−11.0	−7.9	109/110	109; 110
120	CC^LGC^LA		−9.59	−11.19				M	−8.0	−6.1; −5.0; −4.9	101/102; 110/111; 68	110
121	CCC^LGC		−9.22	(−9.72 R2); −9.32	(S)	(S)	(S)		−8.7	(−9.6; −7.7; −7.2; −7.0; −6.0; −6.0)	(261; 102; 160; 286; 98/99; 138/139)	(98/99)

[a]Only probes that bind strongly or moderately to at least one target RNA are shown. [b]Center of binding site according to Figure 1, where the center is the target RNA nucleotide complementary to the third nucleotide from the 5′-end of the probe. [c]In sequence of the modified probe: LNA nucleotides are marked with superscript ^{L}; D represents 2,6-diaminopurine riboside; and nucleotides without a superscript are 2′-*O*-methyl-nucleotides. [d]Calculated for 100 mM NaCl buffer according to a published equation (*15*). [e]Calculated for target RNA which binds the probe. Symbols: S, strong binding; M, medium binding. [f]Other buffer composition: 10 mM Tris-HCl at pH 8.0. [g]Alternative binding sites for Pk2. The predicted values of $\Delta G°_{37}$ for target RNA with no structure include contributions from the first 5′ and 3′ dangling ends. These $\Delta G°_{37}$ values were calculated with the bimolecular mode of RNAstructure 4.6 which assumes that both the target and probe are unmodified RNA. [h]Values and probable binding sites in parentheses consider *B. mori* R2 5′RNA. [i]Values of predicted $\Delta G°_{37}$ and corresponding to them positions of alternative binding sites are arranged in both columns in the same order. (S), strong binding for *B. mori* R2 5′RNA (*15*).

Table 5: Thermodynamic Parameters of RNA Model Motifs in 10 mM NaCl Buffer[a]

RNA (5′ to 3′)	average of curve fits						
	$-\Delta H^\circ$ (kcal/mol)	$-\Delta S^\circ$(eu)	$-\Delta G^\circ_{37}$ (kcal/mol)	T_M (°C)	$\Delta\Delta G^\circ_{37}$ (kcal/mol)	$\Delta\Delta G^\circ_{37}$ (kcal/mol)	$-\Delta G^\circ_4$ (kcal/mol)
H1 GUGACCCAUACUGGUCAC	53.7 ± 1.6	157.5 ± 4.6	4.87 ± 0.20	67.9	0		10.12
H2 GUGACCAAAAAAGGUCAC	56.6 ± 5.5	163.6 ± 16.2	5.85 ± 0.48	72.7		0	11.28
H3 UCUGUGACCCAUACUGGUCAC AGA	75.0 ± 1.5	215.6 ± 4.4	8.15 ± 0.24	74.8			15.44
H4 GUGACCCAUACUGGUCACUUC	61.5 ± 4.8	178.8 ± 14.0	6.04 ± 0.42	70.8	−1.17		11.97
H5 GUGACCAAAAAAGGUCACUUC	63.4 ± 4.9	182.4 ± 14.2	6.83 ± 0.47	74.5		−0.98	12.87
H6 UCUGUGACCCAUACUGGUCAC	54.8 ± 3.1	161.2 ± 9.3	4.81 ± 0.23	66.9	0.06		10.15
H7 UCUGUGACCAAAAAAGGUCAC	55.1 ± 5.8	159.9 ± 17.1	5.48 ± 0.52	71.3		0.37	10.81
B1 CGUGCUCUGUGACCAAAAAAGG UCACGCACG	48.0 ± 2.3	139.8 ± 6.7	4.65 ± 0.23	70.3	0		9.27
B2 CGUGCGUGACCAAAAAAGGUCA CUUCGCACG	68.6 ± 2.3	201.0 ± 6.9	6.24 ± 0.15	68.0	−1.59	0	12.92
B3 CGUGCUCUGUGACCAAAAAAGG UCACGCACGGUG	52.6 ± 1.2	154.2 ± 3.6	4.82 ± 0.14	68.2	−0.18	1.42	9.89
B4 CACCGUGCUCUGUGACCAAAAA AGGUCACGCACGGUG	75.5 ± 4.9	217.8 ± 14.1	7.98 ± 0.54	73.7	−3.33	−1.74	15.17
IL1 CGUGCUCUGUGACCAAAAAAG GUCACUUCGCACG	75.9 ± 3.6	223.2 ± 10.8	6.68 ± 0.34	66.9	0		14.07
IL2 GGUCACUUCGCACGAAAAAAC GUGCUCUGUGACC	101.1 ± 6.2	301.4 ± 18.9	7.64 ± 0.38	62.3	−0.96	0	17.61
IL3 CACCGUGCUCUGUGACCAAAA AAGGUCACUUCGCACGGUG	70.8 ± 4.0	205.1 ± 11.5	7.19 ± 0.44	72.1	−0.51	−0.45	13.99
Pk1 GUGACCUACGCAGCGGUCACU UCAUAGGCUGC	50.4 ± 4.7	147.8 ± 13.8	4.54 ± 0.41	67.7	0		9.46
Pk-H1 GUGACCUACGCAGCGGUCAC	23.6 ± 1.9	70.8 ± 6.0	1.69 ± 0.12	60.8	2.85		3.99
Pk-H2 GCAGCGGUCACUUCAUAGGC UGC	47.6 ± 8.2	143.6 ± 25.5	3.08 ± 0.37	58.5	1.46	0	7.83
Pk-H3 CGCAGCGGUCACUUCAUAGG CUGCG	51.6 ± 4.8	152.9 ± 14.2	4.23 ± 0.41	64.7		−1.15	9.25

[a]Solutions are 10 mM NaCl, 20 mM sodium cacodylate, and 0.5 mM Na_2EDTA at pH 7 (buffer D).

sites 37 and 38. Unexpectedly, medium binding was observed at sites 28 and 34. Hybridization results reveal that 3′-dangling end in B3 barely stabilizes helix II, in comparison to B1, which is consistent with measurements of thermodynamic stability (Table 5). B4 has helix IIa extended by 3 base pairs, which significantly stabilizes helix IIa as demonstrated by hybridization experiments and measurements of the free energy (Figure 1 and Tables 2 and 4). Strong binding sites were noticed in the bulge loop (positions 9 and 11) but also unexpectedly at positions 37 and 38 in helix IIa.

Three RNAs with a 3 × 3 nucleotide internal loop, IL1−IL3, were also studied (Figure 1, Tables 2 and 4). In IL1, the internal loop is accessible for binding at positions 9−11, 30b, and 32. As for B1 and B2, binding sites in IL1 extended to helix II adjacent to the loop. To test this pattern, IL2 contains the same helixes I and II and the internal loop, but loop AAAAAA (loop *c*) closes helix II instead of helix I. As expected, sites accessible to binding are in the internal loop and in helix I instead of helix II. IL3 has helix II extended by three base pairs (IIa) to enhance its thermodynamic stability. Strong or medium binding was noticed at sites 8−13 and 28−34. Unexpected binding was observed at positions 37 and 38, as for B4.

Binding of RNA Pseudoknots to Isoenergetic Microarray Probes. Pk1 was designed to form the pseudoknot structure shown in Figure 2. The binding sites were 7, 8 (strong), and 9 (medium) in loop *d*, and 21−23 (strong) and 24 and 25 (medium) in loop *e*. Strong binding was also observed at sites 6, 19, and 20. Predicted helix III did not bind probes. Hybridization of Pk1 to microarray probes is consistent with the presence of helix III, necessary for pseudoknot formation (Figures 2 and 4, and Table 3).

Pk-H1, Pk-H2, and Pk-H3 have the component hairpins of the Pk1 pseudoknot (Figure 2). In Pk-H1, loop *d* was accessible at sites 8−13, including sites 10−13, which did not bind in pseudoknot Pk1. Helix I displayed moderate binding at sites 16−18, which is similar to hairpin H1 (containing the same helix I) but different from Pk1. Hairpin Pk-H2 bound probes in loop *e* but more sparsely than hairpin Pk-H3. Pk-H3 contains helix IIIa,

Table 6: Thermodynamic Parameters of RNA Model Duplexes[a]

RNA (5′ to 3′)	average of curve fits				T_M^{-1} vs log (C_T/4) plots			
	$-\Delta H°$ (kcal/mol)	$-\Delta S°$ (eu)	$-\Delta G°_{37}$ (kcal/mol)	T_M (°C)	$-\Delta H°$ (kcal/mol)	$-\Delta S°$ (eu)	$-\Delta G°_{37}$ (kcal/mol)	T_M[b] (°C)
bulge mimic UGC UCUGUG	37 $D^MC^LC^MG^LU^MG^L$	52.4 ± 4.3	160.9 ± 15.0	2.45 ± 0.43	14.6	55.3 ± 20.1	171.0 ± 69.9	2.21 ± 1.94	14.5
bulge mimic UGC UCUGUG	38 $C^LD^MC^L$ C^MG^L	55.9 ± 12.4	167.3 ± 41.0	4.02 ± 0.38	23.7	50.7 ± 12.3	149.6 ± 41.3	4.30 ± 0.80	23.9
37 $D^MC^LC^MG^LU^MG^L$	37 $D^MC^LC^MG^LU^MG^L$	55.1 ± 4.3	140.8 ± 12.9	11.40 ± 0.39	73.0	50.5 ± 6.8	127.7 ± 19.9	10.93 ± 0.71	73.0
loop *b* mimic CAAAAAAG	37 $D^MC^LC^MG^LU^MG^L$	44.1 ± 10.6	104.9 ± 30.5	11.52 ± 1.18	76.6	40.6 ± 1.0	95.5 ± 3.0	11.02 ± 0.09	75.5
loop *b* mimic CAAAAAAG	38 $C^LD^MC^LC^MG^L$	16.4 ± 4.1	28.5 ± 13.7	7.51 ± 0.22	56.9	20.8 ± 3.7	43.4 ± 11.9	7.38 ± 0.40	50.1
loop *a* mimic CCAUACUG	25 $G^MD^MC^LC^MA^MG^L$	22.3 ± 6.6	51.8 ± 21.3	6.21 ± 0.54	32.5	17.2 ± 10.4	35.3 ± 33.1	6.26 ± 2.84	32.2
loop *a* mimic CCAUACUG	30a $U^MC^LU^MG^LU^MG^L$	28.8 ± 3.9	72.8 ± 13.6	6.20 ± 0.36	33.5	33.8 ± 5.2	89.8 ± 17.5	5.94 ± 0.29	31.7
25 $G^MD^MC^LC^MA^MG^L$	25 $G^MD^MC^LC^MA^MG^L$	16.8 ± 7.5	36.1 ± 25.2	5.63 ± 0.40	36.1	18.2 ± 8.2	41.8 ± 28.6	5.24 ± 1.41	29.7
30a $U^MC^LU^MG^LU^MG^L$	30a $U^MC^LU^MG^LU^MG^L$	36.9 ± 3.6	100.3 ± 10.9	5.81 ± 0.26	38.1	56.3 ± 14.9	164.6 ± 49.6	5.26 ± 0.62	34.7

[a]Solutions are 1 M NaCl, 20 mM sodium cacodylate, and 0.5 mM Na_2EDTA at pH 7 (buffer C). [b]Calculated for 10^{-4} M total strand concentration. In sequences of oligonucleotides: LNA nucleotides are marked with superscript ^{L}; D represents 2,6-diaminopurine riboside, 2′-*O*-methyl-nucleotides are marked with superscript ^{M}.

extended with an additional CG pair for stability. Sites 18−25 bind indicating open regions of loop *e*.

The results of structural mapping of a more complex pseudoknot, Pk2, are shown in Table 4 and Figure 3. This pseudoknot occurs in the 5′-region of the *B. mori* retrotransposon R2 RNA and is part of a 323 nucleotide fragment that binds to one copy of R2 protein and orchestrates second strand DNA cleavage during the insertion of the R2 sequence into the host genome (*35*−*37*). The pseudoknot structure of Pk2 was deducted from NMR mapping (*29*) and sequence comparison (*15*, *16*). The Pk2 pseudoknot was hybridized to isoenergetic microarrays in conditions previously used for mapping of the 323 nucleotide R2 5′RNA, in 200 mM NaCl and 5 mM $MgCl_2$ (buffer A), and 1 M NaCl and 5 mM $MgCl_2$ (buffer B) at 4 °C or room temperature. Microarray hybridization data in buffer A at room temperature reveals strong binding sites at positions 55, 56, 57, 70, 71, and 110 (numbering according to R2 5′RNA) and medium binding at positions 54, 85, 96, 109, and 113, consistent with the pseudoknot secondary structure. These regions accessible for probes also correspond with enzymatic and chemical mapping (Figure 3 and Table 4), and overall support the pseudoknot structure.

Thermodynamic Measurements. Thermodynamic parameters were measured for short model RNAs (Table 5, Supporting Information). Also, possible alternative duplexes that several probes could form with a part of target RNA were melted (Table 6). Potential alternative duplexes for probes that demonstrate unexpected binding are shown in Figure 5.

DISCUSSION

Binding of short oligonucleotides to target DNA or RNA is crucial for many applications. Examples include primers for extension of the second strand (*38*), strategies based on RNAi phenomena (*39*, *40*), and antisense (*41*) or ribozyme approaches (*42*) to modify gene expression (*21*, *24*, *25*, *43*). To be therapeutics, oligonucleotides must bind strongly and selectively to a complementary fragment of target RNA. Microarray technologies also involve the binding of oligonucleotides to DNA or RNA (*14*−*16*, *44*−*46*).

The secondary structure of any RNA can be considered as the sum of many structural motifs such as single and double stranded fragments, dangling ends, bulges, internal loops, multibranch loops, and pseudoknots. Tertiary interactions of structural motifs, e.g., by coaxial stacking or A-platforms, can affect overall folding of a large RNA as well. Moreover, the formation of RNA complexes with proteins or other biomolecules can influence RNA structure. Nevertheless, isolated structural motifs of RNA provide fundamental models to study the interactions of folded RNA with oligonucleotides. Herein, the binding of hairpins, dangling ends, bulges, internal loops, and pseudoknots to oligonucleotide probes on microarrays was studied. The model RNA structural motifs were constructed by the extension of shorter ones to allow for systematic evaluation of the influence of RNA structure on the hybridization process. The RNA models can be split into two categories: hairpins and pseudoknots. The hairpins contained various loop sequences, different lengths of stems, 5′- or 3′-side trinucleotide dangling ends, bulges, or internal loops (Figure 1). The sequences were designed to minimize as much as possible the alternative binding sites of probes.

Hairpins H1−H7 form one systematic set of structural motifs. Hairpins H1, H3, H4, and H6 have loop sequence 5′CAUACU3′

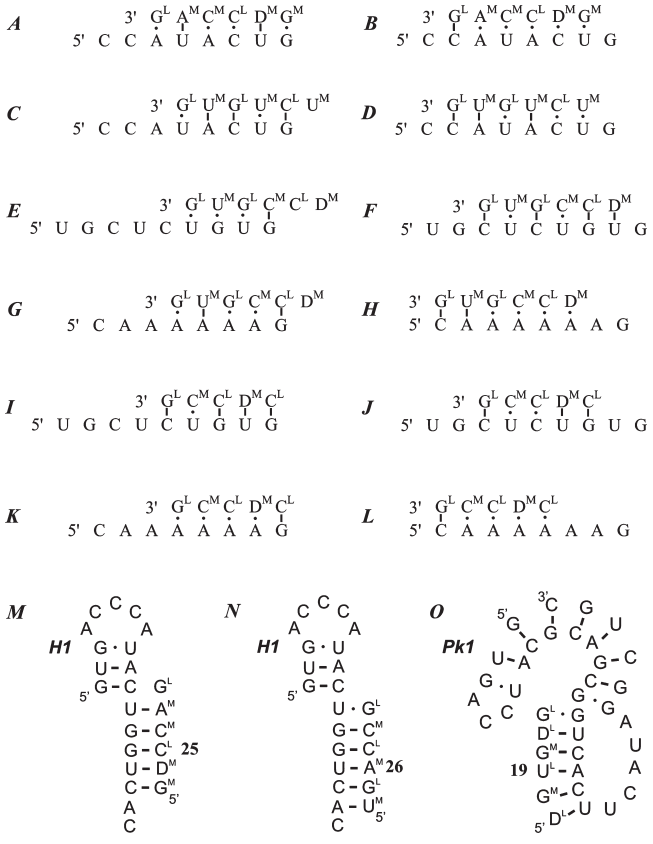

FIGURE 5: Possible alternative duplexes: ***A***, ***B***, alternative binding of probe 25 to loop *a*; ***C***, ***D***, alternative binding of probe 30a to loop *a*; ***E***, ***F***, alternative binding of probe 37 to the bulge of B4; ***G***, ***H***, alternative binding of probe 37 to loop *b*; ***I***, ***J***, alternative binding of probe 38 to the bulge of B4; ***K***, ***L***, alternative binding of probe 38 to loop *b*; ***M***, possible rearrangement of H1 induced by the binding of probe 25; ***N***, possible rearrangement of H1 induced by the binding of probe 26; ***O***, possible rearrangement of Pk1 induced by the binding of probe 19.

(loop *a*), and in most cases, strong or medium binding to that loop was observed. There were particularly strong binding at sites 19−21 because binding to that fragment allows for interactions of loop *a* with almost the entire length of probes. Hairpins H2, H5, and H7 with 5′AAAAAA3′ (loop *b*) were designed to minimize possible probe binding to the loop. The 5′AAAAAA/3′UUUUUU duplex is predicted to have a free energy of 0.34 kcal/mol at 37 °C in standard, 1 M NaCl buffer (C). The different sequences of loops *a* and *b* affect the measured thermodynamic stability (ΔG^{o}_{37}) of both hairpins, which were equal to −4.87 and −5.85 kcal/mol in 10 mM NaCl (buffer D) for hairpins H1 and H2, respectively (Table 5) (*47*−*49*). The hairpin H3 with three extra base pairs was even more stable with measured free energy in buffer D of −8.15 kcal/mol at 37 °C.

Hairpins H1 and H3 unexpectedly bind probes complementary to the helix at position 25, and H3 additionally binds the probe complementary to site 30a (Table 1). Binding of those probes implies the opening helix I or Ia, respectively, or binding to loop *a* with mismatches (Figure 5). To gain insight into the latter possibility, 5′CCAUACUG3′/5′G^{M}D^{M}C^{L}C^{M}A^{M}G^{L}3′ and 5′CCAUACUG3′/5′U^{M}C^{L}U^{M}G^{L}U^{M}G^{L}3′ duplexes (underlined nucleotides are single stranded in model RNA) were melted (Table 6 and Figure 5). Those duplexes mimic possible loop *a*/probe interactions. Moreover, to make melting analysis unambiguous, the possibility of the formation of probe/probe self-associated mismatched duplexes in the solution was analyzed as well. Unfortunately, probes 25 and 30a, both form stable self-associated duplexes. The melting curves of mismatched duplexes formed between 5′CCAUACUG3′ (mimic of loop *a*) and probes 25 and 30a were very broad and noncooperative. Thus, the observed melting curves are likely the result of overlapping of the melts of probe/probe and 5′CCAUACUG3′/probe duplexes (Table 6). This suggests that probes 25 and 30a bind to the loop region either weakly or not at all. Probe 25 possibly binds to H1 and H3 by inducing a complete rearrangement of the hairpin as shown in Figure 5. This rearrangement allows probe 25 to form five or six Watson−Crick base pairs and is further stabilized by a 3′-dangling end A. Moreover the duplex formed can coaxially stack with the stem of the new hairpin. A similar rearrangement would allow probe 26 to bind (Figure 5).

The hairpins H4−H7 were formed by a trinucleotide extension of the 5′- or 3′-side of core hairpins H1 and H2. It is known from thermodynamic measurements that 3′-dangling ends enhance duplex stability and that 5′-dangling ends have little effect (*50*−*57*). The stabilization effects are dependent on the length and sequence of dangling ends as well as on identity and orientation of the adjacent base pair (*1*, *54*, *56*). Comparison of the thermodynamic stability of hairpin H1 with H4 as well as hairpin H2 with H5 demonstrate that the presence of UUC as a 3′-dangling end enhances stabilities ($\Delta\Delta G^{o}_{37}$) by 1.17 and 0.98 kcal/mol, respectively (Table 5). For the hairpins H6 and H7, UCU as a 5′-dangling end does not change the stability more than experimental error, (destabilization by 0.06 and 0.37 kcal/mol, respectively). Those results, particularly the influence of 3′-dangling ends are similar to the literature values (*1*, *55*). The thermodynamic influence of the trinucleotide dangling ends are consistent with the binding of model hairpins H4−H7 to microarray probes. H4 and H5 with trinucleotide 3′-dangling ends strongly bind at position 30b (Figure 1). In the case of hairpin H4, binding to loop *a* was very limited, perhaps because of the competition with the binding to site 30b. Binding of the probes to hairpins H6 and H7 carrying UCU 5′-dangling ends was more extensive than to H4 and H5. For example, probes 11−13 now bind strongly and probes 14−15 moderately. Binding of probes 11−14 is favored by base pairing to the 5′-dangling UCU and coaxial stacking with the rest of the hairpin stem. The medium signal of probe 15 is surprising. It may require a rearrangement of the hairpin.

Structures B1−B4 were formed by extension of hairpins H4−H7 to add a bulge loop to the stem. In B1, binding occurs at position 9 of the bulge loop and at sites 6−8 of helix II, in the strand 5′-adjacent to the bulge loop. In B2, the bulge loop was placed on the opposite side of the stem. Here, binding to probes occurs in the bulge loop (positions 29, 30, and 32) as well as in helix II at positions 33 and 34, 3′-adjacent to the bulge loop. The 1.59 kcal/mol difference in stability ($\Delta\Delta G^{o}_{37}$) of B1 and B2 is significant but does not influence the binding to microarrays (Table 1). To achieve extra stabilization of B1, a GUG 3′-dangling end was added to form B3. The stabilization effect of GUG as the 3′-dangling end, equal to 0.17 kcal/mol, was unexpectedly low. Binding to B3 was similar to that to B1, except that bindings were more extensive (whole bulge region binds strong or medium), and binding to the GUG 3′-dangling end was observed. B4 had an extended helix II called helix IIa. This stabilizes helix II and eliminated binding to the helical strand 5′-adjacent to the bulge loop.

Unexpectedly, strong bindings were noticed for probes 5′D^{M}C^{L}C^{M}G^{L}U^{M}G^{L}3′ and 5′C^{L}D^{M}C^{L}C^{M}G^{L}3′ which are

complementary, respectively, to sites 37 and 38 of B4 and IL3 (Table 2). To confirm the binding of these probes at positions 37 and 38, the possibilities of the alternative binding sites have to be eliminated (Figure 5). For this purpose, UV melting was measured for probes 37 and 38 with 5′UGCUCUGUG3′ and 5′CAAAAAAG3′, which contain the sequences of the bulge loop and hairpin loop *b*, respectively. Again, both probes were checked to see whether they form stable self-associated duplexes. Indeed, probe 37 showed a melting transition (Table 6). Thermodynamic measurements show that duplexes formed by both probes and the bulge loop mimic are rather weak, with free energy at 37 °C equal to −2.45 and −4.02 kcal/mol in 1 M NaCl (buffer C) for 5′UGCUCUGUG3′/5′$D^MC^LC^MG^LU^MG^L$3′ and 5′UGCUCUGUG3′/5′$C^LD^MC^LC^MG^L$3′, respectively, suggesting that such binding does not occur during hybridization. At the same time, duplexes formed by the same probes with the loop *b* mimic, 5′CAAAAAAG3′, were very broad and uncooperative, indicating weak or no binding. Evidently, probes complementary to sites 37 and 38 do not bind to alternative binding sites in loop *b*. Moreover, hybridization of hairpin H5 to microarrays containing probes 5′$D^MC^LC^MG^LU^MG^L$3′ (*37*) and 5′$C^LD^MC^LC^MG^L$3′ (*38*), complementary, respectively, to positions 37 and 38 in bulge B4, showed no binding to loop *b*. Probably, the binding of probes 37 and 38 involves favorable rearrangement of RNA structure. The other possibility besides the opening of helix IIa is the formation of base triples by probe 37 and 38.

IL1 is similar in structure to B1 except that single stranded UUC was added on the other side of the helical stem to form an internal loop. IL2 was formed by switching the position of hairpin loop 5′AAAAAA3′ from the end of helix I to helix II. IL3 has a structure similar to IL1, but helix II was extended by three extra base pairs (helix IIa) to increase thermodynamic stability. For IL1, the binding of isoenergetic probes was similar to the sum of binding to B1 and B2. Binding was observed at the internal loop (positions 9−11 and 30, and 32) and at helix II adjacent to the internal loop (sites 6−8 and 33−35). The hybridization results were very interesting for internal loop IL2, in which the hairpin loop terminates helix II instead of helix I. Predicted free energy for helix I and II alone were −8.1 and −6.0 kcal/mol in 1 M NaCl (buffer C), respectively. The results of IL2 probe binding clearly demonstrate that the terminal helix was partially accessible for the binding of microarray probes. Evidently, the position of a stem in the molecule is more important than its thermodynamic stability. However, as seen for IL3, the significant extension of closing blunt ended helix IIa limits the binding of probes to a terminal stem.

Two pseudoknots were studied: Pk1 with 32 nucleotides and Pk2 with 74 nucleotides. The latter is found in *B. mori* R2 retrotransposon 5′RNA (*15*, *16*, *29*).

Hybridization analysis of Pk1 is consistent with the existence of helix III, part of the pseudoknot (Figure 2). Strong and medium bindings were found at positions 6−9 and 19−25 in single stranded fragments and adjacent base pairs expected in the pseudoknot structure. Hybridization results for Pk1 indicated that nucleotides 10−14 and 28−32 are inaccessible for microarray probes, suggesting that this region is involved in base pairing to form the pseudoknot structure. As a control, binding to sites 10−13 was observed for hairpin Pk-H2. Binding of probe 19 in the terminal stem is surprising but may also be due to the rearrangement of base pairing in a terminal stem as suggested in Figure 5.

The thermodynamic stability (ΔG^{o}_{37}) in 10 mM NaCl (buffer D) of pseudoknot Pk1 and hairpins, Pk-H1 and Pk-H2, which are components of Pk1 were −4.54, −1.69, and −3.08 kcal/mol, respectively. As expected, Pk1 is more stable than individual hairpins Pk-H1 and Pk-H2.

Hybridization to Pk2 alone can be compared to that when it is part of the entire 323 nucleotide R2 5′RNA (*15*) (Table 4 and Figure 3). For pseudoknot Pk2, strong and medium binding was observed at regions of single strand or loop closing nucleotides 54−57, 70, 71, 85, 96, 109, 110, and 113. Results of microarray mapping were confirmed by chemical and enzymatic mapping as well as digestion with lead. When hybridization was measured on R2 5′RNA, binding was limited to positions 56, 70, 71, 98, and 99. Binding to 98 and 99 was not observed during the hybridization of Pk2 alone.

The loop fragments 107−114 are more available for binding in pseudoknot Pk2 than in the entire R2 5′RNA. The same observation concerns the chemical mapping of Pk2 alone rather than as part of R2 5′RNA. More probes and stronger binding were noticed for Pk2 in 1 M NaCl and 5 mM $MgCl_2$ (buffer B) than in 200 mM NaCl and 5 mM $MgCl_2$ (buffer A), especially in loop 107−114. The region which is more accessible in 1 M NaCl (buffer B) is distinctively cleaved by Pb^{2+}. The loops of Pk2 pseudoknot are clearly accessible for probe binding as well as chemicals and enzymes. Differences in probe binding and mapping of Pk2 alone and as part of R2 5′RNA presumably reflect tertiary interactions that occur in R2 5′RNA and/or in Pk2.

The microarray results on pseudoknot Pk2 are consistent with NMR data for Pk2 (*29*). Imino proton spectra coupled with free energy minimization identified stable helixes G37-U42/A66-C71 and A43-C45/G50-U52. These regions are also unavailable for binding probes both in Pk2 and the whole R2 5′RNA. The binding in all tested conditions confirmed the proposed structure of pseudoknot Pk2.

The analysis of RNA structural motifs binding to microarray probes demonstrate the following features: (i) bulges, internal loops, and dangling ends bind strongly to microarray probes; (ii) a terminal stem can also bind strongly, possibly due to the rearrangement of base pairs; and (iii) an internal stem does not bind strongly. Moreover, some unexpected binding sites could be the result of alternative binding of probes to a single stranded fragment of target RNA. The results suggest that microarray binding may not easily provide constraints for mapping RNA secondary structure but can rapidly provide data to test proposed structures. Simultaneously using constraints from various methods (chemical, enzymatic, and microarray mapping) with energy minimization programs provides optimal results (*16*).

It seems that longer RNAs are better targets for microarray analysis because of their larger overall stabilities. The data presented here demonstrates that the location of the structural motif in the context of the whole structure of target RNA and both secondary and tertiary interactions influence the accessibility of RNA to probe binding. Moreover, a very careful analysis of alternative binding sites is very important.

ACKNOWLEDGMENT

I thank Dr. Douglas H. Turner for reading the manuscript and for helpful discussions.

SUPPORTING INFORMATION AVAILABLE

Complete tables with hybridization results and examples of melting curves. This material is available free of charge via the Internet at http://pubs.acs.org.

REFERENCES

1. Turner, D. H. (2000) Conformational Changes, in Nucleic Acids: Structures, Properties and Functions (Bloomfield, V. A., Crothers, D. M., and Tinoco, I., Eds.) pp 259−334, University Science Books, Sausalito, CA.
2. Kurreck, J., Wyszko, E., Gillen, C., and Erdmann, V. A. (2002) Design of antisense oligonucleotides stabilized by locked nucleic acids. *Nucleic Acids Res. 30*, 1911–1918.
3. Freier, S. M., and Altmann, K.-H. (1997) The ups and downs of nucleic acid duplex stability: structure−stability studies on chemically-modified DNA:RNA duplexes. *Nucleic Acids Res. 25*, 4429–4443.
4. Wengel, J., Petersen, M., Frieden, M., and Koch, T. (2003) Chemistry of locked nucleic acids (LNA): Design, synthesis, and biophysical properties. *Lett. Pept. Sci. 10*, 237–253.
5. Xia, T. B., SantaLucia, J., Burkard, M. E., Kierzek, R., Schroeder, S. J., Jiao, X. Q., Cox, C., and Turner, D. H. (1998) Thermodynamic parameters for an expanded nearest-neighbor model for formation of RNA duplexes with Watson-Crick base pairs. *Biochemistry 37*, 14719–14735.
6. Freier, S. M., Kierzek, R., Jaeger, J. A., Sugimoto, N., Caruthers, M. H., Neilson, T., and Turner, D. H. (1986) Improved free-energy parameters for predictions of RNA duplex stability. *Proc. Natl. Acad. Sci. U.S.A. 83*, 9373–9377.
7. SantaLucia, J., Allawi, H. T., and Seneviratne, A. (1996) Improved nearest-neighbor parameters for predicting DNA duplex stability. *Biochemistry 35*, 3555–3562.
8. Sugimoto, N., Nakano, S., Katoh, M., Matsumura, A., Nakamuta, H., Ohmichi, T., Yoneyama, M., and Sasaki, M. (1995) Thermodynamic parameters to predict stability of RNA/DNA hybrid duplexes. *Biochemistry 34*, 11211–11216.
9. Kierzek, E., Mathews, D. H., Ciesielska, A., Turner, D. H., and Kierzek, R. (2006) Nearest neighbor parameters for Watson-Crick complementary heteroduplexes formed between 2′-O-methyl RNA and RNA oligonucleotides. *Nucleic Acids Res. 34*, 3609–3614.
10. McTigue, P. M., Peterson, R. J., and Kahn, J. D. (2004) Sequence-dependent thermodynamic parameters; for locked nucleic acid (LNA)-DNA duplex formation. *Biochemistry 43*, 5388–5405.
11. Pasternak, A., Kierzek, E., Pasternak, K., Turner, D. H., and Kierzek, R. (2007) A chemical synthesis of LNA-2,6-diaminopurine riboside, and the influence of 2′-O-methyl-2,6-diaminopurine and LNA-2,6-diaminopurine ribosides on the thermodynamic properties of 2′-O-methyl RNA/RNA heteroduplexes. *Nucleic Acids Res. 35*, 4055–4063.
12. Kierzek, E., Ciesielska, A., Pasternak, K., Mathews, D. H., Turner, D. H., and Kierzek, R. (2005) The influence of locked nucleic acid residues on the thermodynamic properties of 2′-O-methyl RNA/RNA heteroduplexes. *Nucleic Acids Res. 33*, 5082–5093.
13. Mathews, D. H., Disney, M. D., Childs, J. L., Schroeder, S. J., Zuker, M., and Turner, D. H. (2004) Incorporating chemical modification constraints into a dynamic programming algorithm for prediction of RNA secondary structure. *Proc. Natl. Acad. Sci. U.S.A. 101*, 7287–7292.
14. Kierzek, E., Kierzek, R., Turner, D. H., and Catrina, I. E. (2006) Facilitating RNA structure prediction with microarrays. *Biochemistry 45*, 581–593.
15. Kierzek, E., Kierzek, R., Moss, W. N., Christensen, S. M., Eickbush, T. H., and Turner, D. H. (2008) Isoenergetic penta- and hexanucleotide microarray probing and chemical mapping provide a secondary structure model for an RNA element orchestrating R2 retrotransposon protein function. *Nucleic Acids Res. 36*, 1770–1782.
16. Kierzek, E., Christensen, S. M., Eickbush, T. H., Kierzek, R., Turner, D. H., and Moss, W. N. (2009) Secondary structures for 5′ regions of R2 retrotransposon RNAs reveal a novel conserved pseudoknot and regions that evolve under different constraints. *J. Mol. Biol. 390*, 428–442.
17. Kierzek, E., Fratczak, A., Pasternak, A., Turner, D. H., Kierzek, R. (2007) Isoenergetic RNA microarrays, a new method to study the structure and interactions of RNA, in 2nd European Conference on Chemistry for Life Sciences, Wroclaw , pp 25−30, Medimond, International Proceedings Division, Bologna, Italy.
18. Pasternak, A., Kierzek, E., Pasternak, K., Fratczak, A., Turner, D. H., and Kierzek, R. (2008) The thermodynamics of 3′-terminal pyrene and guanosine for the design of isoenergetic 2′-O-methyl-RNA-LNA chimeric oligonucleotide probes of RNA structure. *Biochemistry 47*, 1249–1258.
19. Jenek, M., and Kierzek, E. (2008) Isoenergetic microarray mapping: the advantage of this method in studying the structure of Saccharomyces cerevisiae $tRNA^{Phe}$. *Nucleic Acids Symp. Ser. 52*, 219–220.
20. Kierzek, E., Barciszewska, M. Z., and Barciszewski, J. (2008) Isoenergetic microarray mapping reveals differences in structure between $tRNA_i^{Met}$ and $tRNA_m^{Met}$ from Lupinus luteus. *Nucleic Acids Symp. Ser. 52*, 215–216.
21. Hackermuller, J., Meisner, N. C., Auer, M., Jaritz, M., and Stadler, P. F. (2005) The effect of RNA secondary structures on RNA-ligand binding and the modifier RNA mechanism: a quantitative model. *Gene 345*, 3–12.
22. Moody, E. M., Lecomte, J. T. J., and Bevilacqua, P. C. (2005) Linkage between proton binding and folding in RNA: A thermodynamic framework and its experimental application for investigating pK(a) shifting. *RNA-Publ. RNA Soc. 11*, 157–172.
23. Matveeva, O. V., Shabalina, S. A., Nemtsov, V. A., Tsodikov, A. D., Gesteland, R. F., and Atkins, J. F. (2003) Thermodynamic calculations and statistical correlations for oligo-probes design. *Nucleic Acids Res. 31*, 4211–4217.
24. Walton, S. P., Stephanopoulos, G. N., Yarmush, M. L., and Roth, C. M. (2002) Thermodynamic and kinetic characterization of antisense oligodeoxynucleotide binding to a structured mRNA. *Biophys. J. 82*, 366–377.
25. Majlessi, M., Nelson, N. C., and Becker, M. M. (1998) Advantages of 2′-O-methyl oligoribonucleotide probes for detecting RNA targets. *Nucleic Acids Res. 26*, 2224–2229.
26. McBride, L. J., and Caruthers, M. H. (1983) An investigation of several deoxyribonucleoside phosphoramidites useful for synthesizing deoxyoligonucleotides. *Tetrahedron Lett. 24*, 245–248.
27. Pedersen, D. S., Rosenbohm, C., and Koch, T. (2002) Preparation of LNA phosphoramidites. *Synthesis* 802–808.
28. Puglisi, J. D., and Tinoco, I. (1989) Absorbency melting curves of RNA. *Methods Enzymol. 180*, 304–325.
29. Hart, J. M., Kennedy, S. D., Mathews, D. H., and Turner, D. H. (2008) NMR-assisted prediction of RNA secondary structure: Identification of a probable pseudoknot in the coding region of an R2 retrotransposon. *J. Am. Chem. Soc. 130*, 10233–10239.
30. Afanassiev, V., Hanemann, V., and Wolfl, S. (2000) Preparation of DNA and protein micro arrays on glass slides coated with an agarose film. *Nucleic Acids Res. 28*, e66.
31. McDowell, J. A., and Turner, D. H. (1996) Investigation of the structural basis for thermodynamic stabilities of tandem GU mismatches: Solution structure of $(rGAGGUCUC)_2$ by two-dimensional NMR and simulated annealing. *Biochemistry 35*, 14077–14089.
32. Merino, E. J., Wilkinson, K. A., Coughlan, J. L., and Weeks, K. M. (2005) RNA structure analysis at single nucleotide resolution by selective 2′-hydroxyl acylation and primer extension (SHAPE). *J. Am. Chem. Soc. 127*, 4223–4231.
33. Ziehler, W. A., and Engelke, D. R. (2000) Probing RNA structure with chemical reagents and enzymes. *Curr. Protoc. Nucleic Acid Chem. 2*, 6.1.1–6.1.21.
34. Ciesiolka, J., Wrzesinski, J., Gornicki, J., Podkowinski, J., and Krzyzosiak, W. J. (1989) Analysis of magnesium, europium and lead binding sites in methionine initiator and elongator tRNAs by specific metal-ion-induced cleavages. *Eur. J. Biochem. 186*, 71–77.
35. Christensen, S. M., and Eickbush, T. H. (2005) R2 target-primed reverse transcription: Ordered cleavage and polymerization steps by protein subunits asymmetrically bound to the target DNA. *Mol. Cell. Biol. 25*, 6617–6628.
36. Christensen, S. M., Ye, J. Q., and Eickbush, T. H. (2006) RNA from the 5′ end of the R2 retrotransposon controls R2 protein binding to and cleavage of its DNA target site. *Proc. Natl. Acad. Sci. U.S.A. 103*, 17602–17607.
37. Eickbush, T. H., and Eickbush, D. G. (2007) Finely orchestrated movements: Evolution of the ribosomal RNA genes. *Genetics 175*, 477–485.
38. Fratczak, A., Kierzek, R., and Kierzek, E. (2009) LNA-modified primers drastically improve hybridization to target RNA and reverse transcription. *Biochemistry 48*, 514–516.
39. Hannon, G. J. (2002) RNA interference. *Nature 418*, 244–251.
40. McManus, M. T., and Sharp, P. A. (2002) Gene silencing in mammals by small interfering RNAs. *Nat. Rev. Genet. 3*, 737–747.
41. Kurreck, J. (2003) Antisense technologies. Improvement through novel chemical modifications. *Eur. J. Biochem. 270*, 1628–1644.
42. Doudna, J. A., and Cech, T. R. (2002) The chemical repertoire of natural ribozymes. *Nature 418*, 222–228.
43. Wrzesinski, J., Legiewicz, M., and Ciesiolka, J. (2000) Mapping of accessible sites for oligonucleotide hybridization on hepatitis delta virus ribozymes. *Nucleic Acids Res. 28*, 1785–1793.

44. Ooms, M., Verhoef, K., Southern, E. M., Huthoff, H., and Berkhout, B. (2004) Probing alternative foldings of the HIV-1 leader RNA by antisense oligonucleotide scanning arrays. *Nucleic Acids Res. 32*, 819–827.
45. Mir, K. U., and Southern, E. M. (1999) Determining the influence of structure on hybridization using oligonucleotide arrays. *Nat. Biotechnol. 17*, 788–792.
46. Sohail, M., Akhtar, S., and Southern, E. M. (1999) The folding of large RNAs studied by hybridization to arrays of complementary oligonucleotides. *RNA-Publ. RNA Soc. 5*, 646–655.
47. Serra, M. J., Barnes, T. W., Betschart, K., Gutierrez, M. J., Sprouse, K. J., Riley, C. K., Stewart, L., and Temel, R. E. (1997) Improved parameters for the prediction of RNA hairpin stability. *Biochemistry 36*, 4844–4851.
48. Serra, M. J., Lyttle, M. H., Axenson, T. J., Schadt, C. A., and Turner, D. H. (1993) RNA hairpin loop stability depends on closing base pair. *Nucleic Acids Res. 21*, 3845–3849.
49. Vecenie, C. J., and Serra, M. J. (2004) Stability of RNA hairpin loops closed by AU base pairs. *Biochemistry 43*, 11813–11817.
50. Freier, S. M., Alkema, D., Sinclair, A., Neilson, T., and Turner, D. H. (1985) Contributions of dangling end stacking and terminal base pair formation to the stabilities of XGGCCp, XCCGGp, XGGCCYp, and XCCGGYp helixes. *Biochemistry 24*, 4533–4539.
51. Freier, S. M., Burger, B. J., Alkema, D., Neilson, T., and Turner, D. H. (1983) Effects of 3′-dangling end stacking on the stability of GGCC and CCGG double helices. *Biochemistry 22*, 6198–6206.
52. Sugimoto, N., Kierzek, R., and Turner, D. H. (1987) Sequence dependence for the energetics of dangling ends and terminal base pairs in ribonucleic-acid. *Biochemistry 26*, 4554–4558.
53. Bibillo, A., Figlerowicz, M., Ziomek, K., and Kierzek, R. (2000) The nonenzymatic hydrolysis of oligoribonucleotides VII. Structural elements affecting hydrolysis. *Nucleosides, Nucleotides Nucleic Acids 19*, 977–994.
54. Ohmichi, T., Nakano, S., Miyoshi, D., and Sugimoto, N. (2002) Long RNA dangling end has large energetic contribution to duplex stability. *J. Am. Chem. Soc. 124*, 10367–10372.
55. Clanton-Arrowood, K., McGurk, J., and Schroeder, S. J. (2008) 3′ Terminal nucleotides determine thermodynamic stabilities of mismatches at the ends of RNA helices. *Biochemistry 47*, 13418–13427.
56. Miller, S., Jones, L. E., Giovannitti, K., Piper, D., and Serra, M. J. (2008) Thermodynamic analysis of 5′ and 3′ single- and 3′ double-nucleotide overhangs neighboring wobble terminal base pairs. *Nucleic Acids Res. 36*, 5652–5659.
57. Liu, J. D., Zhao, L., and Xia, T. B. (2008) The dynamic structural basis of differential enhancement of conformational stability by 5′- and 3′-dangling ends in RNA. *Biochemistry 47*, 5962–5975.